Journal of Power Sources 238 (2013) 103–108

Contents lists available at SciVerse ScienceDirect

Journal of Power Sources

journal homepage: www.elsevier.com/locate/jpowsour

Short communication

Electrochemical behaviour of titanium/iridium(IV) oxide: Tantalum pentoxide and graphite for application in vanadium redox flow battery

Subash Chandrabose Raghu [a,*], Mani Ulaganathan [b], Tuti Mariana Lim [a,c], Maria Skyllas Kazacos [d]

[a] School of Civil and Environmental Engineering, Nanyang Technological University, Block N1, Nanyang Avenue, Singapore 639798, Singapore
[b] Energy Research Institute, Nanyang Technological University, Research Techno Plaza, 50 Nanyang Drive, Singapore 637553, Singapore
[c] School of Life Sciences and Chemical Technology, Ngee Ann Polytechnic, Singapore 599489, Singapore
[d] School of Chemical Engineering, The University of New South Wales, UNSW Sydney, NSW 2052, Australia

HIGHLIGHTS

- VRFB cell has been constructed and the electrochemical performances have been studied.
- V^{3+} to V^{4+} electron transfer state has been obtained.
- Dimensionally stable electro materials Ti/IrO_2:Ta_2O_5 are prepared and studied.
- Energy density 33 Wh L^{-1} has been achieved for DSA electrodes.
- The columbic, voltage and energy efficiencies of Ti/IrO_2:Ta_2O_5 have been estimated and compared with graphite electrode.

GRAPHICAL ABSTRACT

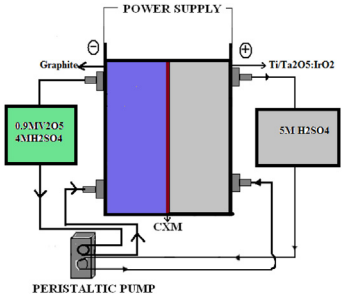

ARTICLE INFO

Article history:
Received 21 January 2013
Received in revised form
1 March 2013
Accepted 6 March 2013
Available online 26 March 2013

Keywords:
Tantalum oxide
Iridium oxide
Vanadium redox flow battery
Dimensionally stable anode
Energy density
Cyclic voltammetry

ABSTRACT

The present work describes the preparation and electrochemical characterisation of titanium/iridium(IV) oxide: tantalum pentoxide (Ti/IrO_2:Ta_2O_5) electrodes for vanadium redox flow battery applications. The electrode surface morphology is examined by field-emission scanning electron microscopy, and their electrochemical behaviours are studied by cyclic voltammetry, chronoamperometry and electrochemical impedance spectroscopy. A charge–discharge study has been performed at different current densities using vanadium sulphate as an electrolyte medium (1.7 M $V^{3.5+}$ and 4 M H_2SO_4), and as-prepared Ti/IrO_2:Ta_2O_5 and pristine graphite are used as the anode and cathode, respectively. To better understand the behaviour of the electrodes and for comparison, a vanadium redox flow battery is also constructed using graphite as the anode as well as the cathode, and its charge–discharge performance is examined. The electrochemical study revealed that the Ti/IrO_2:Ta_2O_5 electrodes exhibit slightly higher catalytic activity and long-term stability than the graphite electrode in highly concentrated sulphuric acid medium. The Ti/IrO_2:Ta_2O_5 electrodes also exhibit slightly higher energy density (33 Wh L^{-1}) than the graphite electrode (31.5 Wh L^{-1}). However, the energy efficiency of Ti/IrO_2:Ta_2O_5 electrode at 40 mA cm^{-2} is 81%, which is lower than that of the graphite electrode (86% at 40 mA cm^{-2}).

* Corresponding author. Tel.: +65 96115376; fax: +65 68622433.
E-mail address: subraghu_0612@yahoo.co.in (S. Chandrabose Raghu).

0378-7753/$ – see front matter © 2013 Elsevier B.V. All rights reserved.
http://dx.doi.org/10.1016/j.jpowsour.2013.03.084

1. Introduction

All-vanadium redox flow batteries (VRFBs) are effective energy-storage systems that were proposed and have been investigated extensively by Skyllas-Kazacos et al. [1–4]. It is expected that energy storage systems will play a more prominent role in bridging the gap between current technology and a clean sustainable future in grid reliability and utilization. Redox flow battery technology is a leading approach in providing a well-balanced solution for current challenges [5]. VRFB is an electrochemical energy storage device in which energy is stored and converted through the chemical changes of a species dissolved in a working fluid [6,7]. V^{5+}/V^{4+} and V^{2+}/V^{3+} redox couples in sulphuric acid were used as positive and negative half-cell electrolytes, respectively, and the cell exhibited an open-circuit voltage of 1.26 V in the 100% charged state [8,9]. Under the overcharge condition, O_2 and CO_2 gases were formed at the anode and H_2 gas was generated at the cathode, which reduced the overall cell performance. To overcome these critical issues, to date, various modifications have made to the electrode materials [10,11]. Special attentions have been paid to the use of graphite fibres with different approaches and various metal compounds to induce modifications. Among them, very few modifications have provided improved electrocatalytic activity for vanadium redox couples and stability in an acidic vanadium solution. Sun et al. [12] reported chemically modified graphite fibres for VRFB applications by impregnating graphite fibres in solutions containing Pt^{4+}, Pd^{2+}, Au^{4+}, Ir^{3+}, and other elements. However, it was found that the electrode modified using Ir^{3+} exhibited the best electrocatalytic behaviour as a vanadium redox couple in H_2SO_4.

Dimensional stable anodes (DSA) are widely used in industrial electrochemical processes. Rychcik et al. [13] tried to modify DSA with IrO_2; the modified material showed good stability and reversibility in a VRFB anode electrode. Fabjan et al. [14] showed that a Ru (-dioxide)-modified carbon fabric electrode showed good performance in a VRFB anode electrode towards the redox reaction of V^{5+}/V^{4+}. Nevertheless, graphite-based electrodes still exhibit poor cyclability over long operation periods due to the erosion of the surface of graphite which is caused for the formation of CO_2 gas. This issue represents a significant challenge in developing suitable anode electrode materials for VRFB applications.

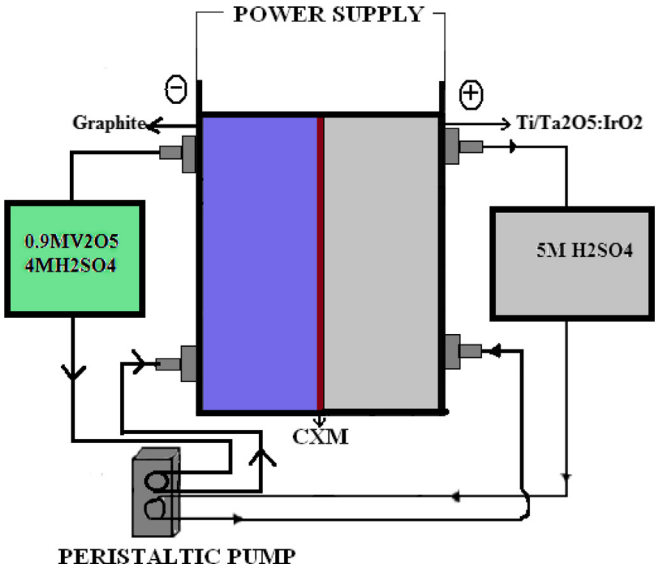

Fig. 1. The electrochemical cell set up used for the preparation of vanadium electrolyte.

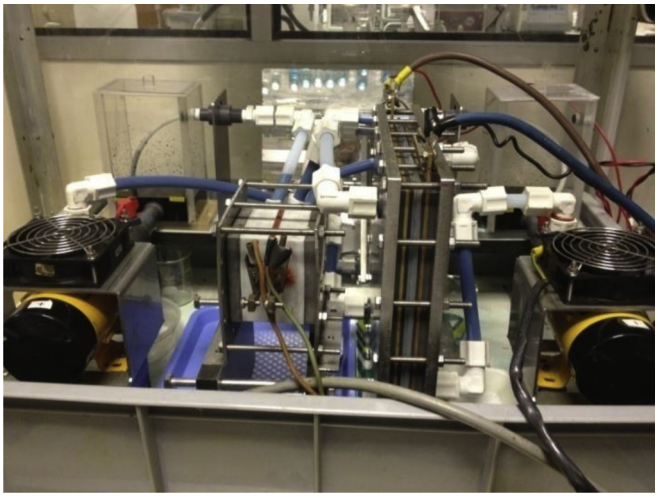

Fig. 2. The laboratory scale VRFB set up used in the present study.

The present work is mainly focused on the preparation and electrochemical analysis of Ti/IrO_2:Ta_2O_5 electrodes for vanadium redox flow systems. The prepared electrode materials are subjected to field-emission scanning electron microscopy (FESEM),

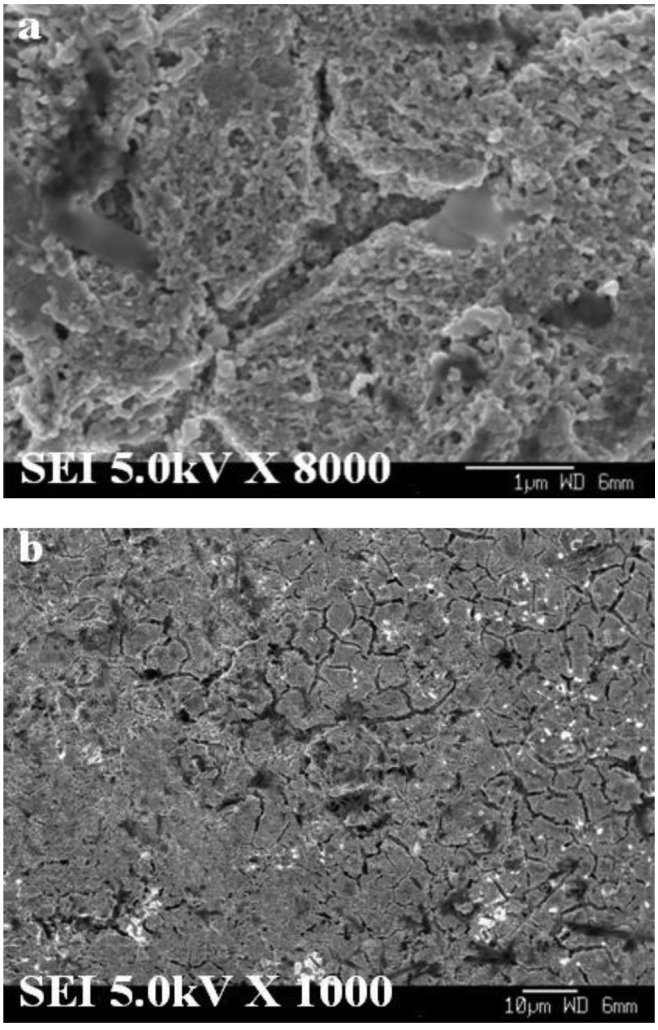

Fig. 3. SEM images of Ti/:IrO_2:Ta_2O_5 electrode at two different magnifications.

cyclic voltammetry (CV), chronoamperometry and electrochemical impedance spectroscopy (EIS) studies. In addition, the charge–discharge profiles of the electrodes have been obtained at different current densities in an optimised vanadium electrolyte medium (2 M $V^{3.5+}$ and 4 M H_2SO_4) using Ti/IrO_2:Ta_2O_5 and graphite as the anode and cathode, respectively. The obtained results for the above mentioned system have also been compared with the VRFB system constructed using pristine graphite as both anode and cathode.

2. Experimental section

All reagents used were of analytical grade: vanadium pentoxide (Alfa Aesar, 99.2%), sulphuric acid (Fisher scientific, 96%), $IrCl_3.H_2O$ (Alfa Aesar, 99.9%), tantalum(V) chloride (Alfa Aesar, 99.9%), isopropanol (Alfa Aesar, 100%) and titanium plate (Purity 99.6%).

2.1. Preparation of Ti/IrO_2:Ta_2O_5 electrode

Titanium plates were sandblasted to produce a rough surface. Then, they were thoroughly cleaned and degreased with acetone, washed with triple-distilled water and etched in oxalic acid (10%) at 80 °C for 1 h. After the etching process, the substrates were washed thoroughly and repeatedly with triple-distilled water and finally air dried. A 70% mole ratio of iridium(III) chloride and 30% mol ratio of tantalum (V) chloride were dissolved in isopropanol. The prepared solution was sprayed or brushed on the titanium substrates and dried at 80 °C. The substrates were then heated to 380–500 °C to thermally decompose iridium and tantalum, then cooled to room temperature. The procedure was repeated 8–12 times, and finally, a post-heat treatment was carried out for 2 h at 500 °C [15–20]. The morphology of the prepared Ti/IrO_2:Ta_2O_5 electrode was observed by field-emission scanning electron microscopy (FESEM) (JSM-6340F, JEOL).

2.2. Electrochemical analysis

Cyclic voltammetry and chronoamperometry analyses were carried out using a three-electrode electrochemical cell on a Solartron Electrochemical Instrument (Sol-1470E, Solartron (UK)). An electrochemically synthesised 1.7 M vanadium ion solution containing 4 M sulphuric acid was used as the electrolyte for the electrochemical analysis experiments. Graphite and Ti/:IrO_2:Ta_2O_5 electrodes with a surface area of 1 cm^2 were used. All potentials were measured using a platinum wire and Ag/AgCl electrodes as counter and reference electrodes, respectively. Cyclic voltammetry (CV) was performed in the potential range from −1.2 V to +1.5 V at different scan rates. CV study was used to evaluate the catalytic activity and performance of the electrodes in a highly concentrated vanadium electrolyte. Electrochemical impedance spectroscopy (EIS) was performed using a CH electrochemical analyser (CH-604D). EIS measurements were carried out using a 1 mV AC voltage signal over the frequency range of 100 kHz–10 mHz.

2.3. Electrolytic preparation of vanadium electrolyte

The electrochemical cell design that was used to prepare vanadium electrolyte is shown in Fig. 1. The electrochemical cell

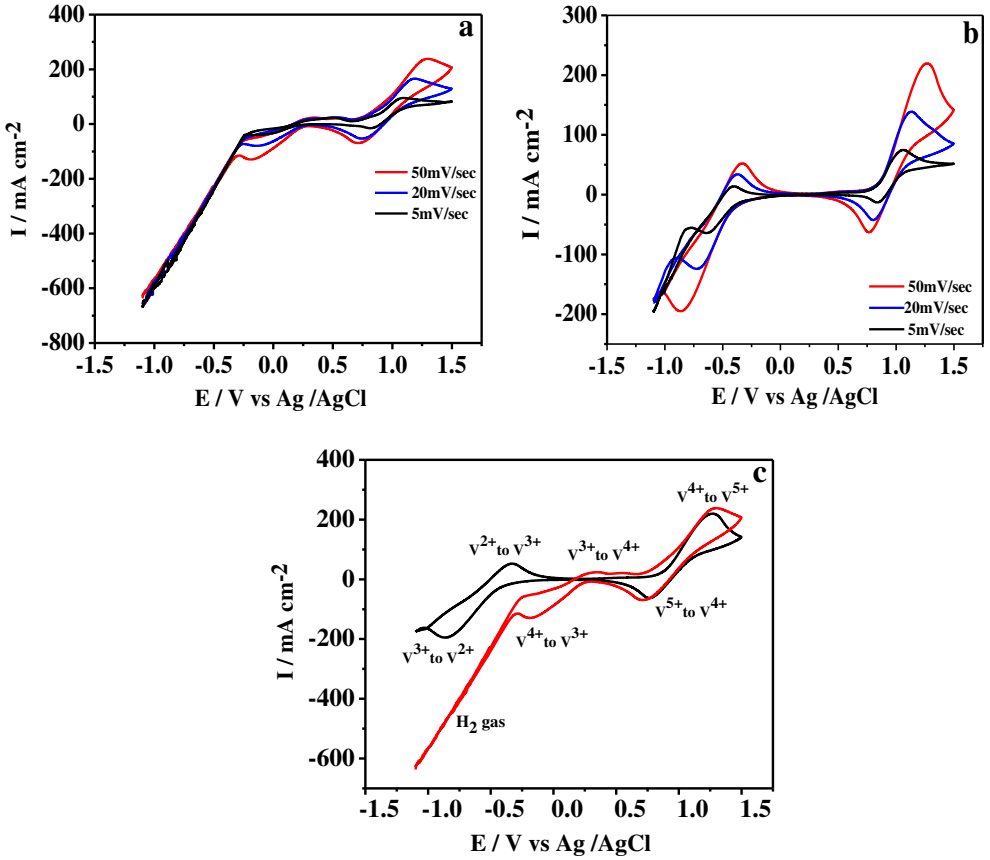

Fig. 4. The cyclic voltammetry behaviour of the graphite and Ti/:IrO_2:Ta_2O_5 electrodes at different scan rates of a) 5; b) 20 and c) 50 mV s^{-1} were carried out by employing 1.7 M $V^{3.5+}$ solution containing 4 M H_2SO_4.

consisted of a titanium plate measuring 100 cm^2 as the anode coated with Ti/IrO_2:Ta_2O_5; a graphite plate measuring 100 cm^2 was used as the cathode. The cell was separated into two compartments by a cation-selective Nafion 117 membrane, with a distance of 1.5 cm between the electrodes. Furthermore, all components were fixed between PVC frames with gaskets. There were two compartments in the electrolytic cell. The anolyte compartment contained a 1 L capacity of 5 M H_2SO_4, and the catholyte compartment contained a 1 L capacity of 0.85 M V_2O_5 and 4 M H_2SO_4 solution. Both compartments were connected to a peristaltic pump using silicone rubber tubes to circulate each solution through the cell. The cell was connected to a 10 A and 15 V DC regulated power supply. Electrolysis was carried out at constant current density of 2.5 A cm^{-2}. During the electrolysis, the sulphate ion concentration was held constant. Samples were collected at various time intervals and subjected to potentiometric analysis to determine the oxidation state of the vanadium ions (4, 3 and 2).

2.4. Vanadium redox flow battery (VRFB)

To evaluate the performance of the Ti/IrO_2:Ta_2O_5 electrode in the VRFB, charge–discharge tests were performed at current densities of 40, 50, 60 70, 80 and 85 mA cm^{-2}. The electrolyte solution used in the VRFB cell consisted of 1.7 M $V^{3.5+}$ in a supporting electrolyte of 4 M H_2SO_4. The laboratory-scale VRFB single cell set-up is shown in Fig. 2. It features a single cell, two electrolyte tanks and two separate pumps. The single cell was composed of 10 cm × 15 cm × 0.5 cm PAN-based graphite felt electrodes (Golden Energy Fuel Cell Co., Ltd., China) in each half-cell, which were compressed against a graphite plate (Golden Energy Fuel Cell Co., Ltd., China) or Ti/IrO_2:Ta_2O_5 electrodes measuring 0.3 cm in thickness. Copper plates were used as current collectors and covered by graphite or TiO_2/IrO_2:Ta_2O_5 electrodes to avoid contact with the electrolyte. The electrolyte was circulated through the cell via flow frames with a 0.3 cm cavity, which contained the porous graphite felt electrodes. A Nafion 117 (DuPont, USA) membrane was used as a separator between the two half-cells. Two stainless steel end plates were bolted together to compress the cell components. Clear Teflon tubes were used to connect the electrolyte solution reservoirs to the pumps and the cell. Another small flow cell with dimensions of 2 cm × 2 cm × 0.5 cm was employed to measure the open-circuit voltage (OCV) of the VRFB. The cell had the same configuration as the VRFB cell. The positive and negative electrolyte inlets of the OCV cell were connected to the positive and negative electrolyte outlets of the VRFB single-cell set-up, respectively. No DC current was applied at the OCV of the cell. Constant current charge–discharge tests were carried out on a custom-designed battery testing system (Developed by SEMIPXI Pte. Ltd., Singapore). Control software was used to control the charge–discharge cycling of the VRFB cell between the set upper charge OCV limit and lower discharge OCV limit and record data related to the measured OCV of the small cell, the voltage of the VRFB cell and the cycling efficiency of the VRFB cell automatically. Unless otherwise specified, all experiments were carried out with an upper charge OCV limit of 1.5 V and lower discharge OCV limit of 1.3 V. The cell columbic efficiency is defined as the discharge capacity divided by the charge capacity and the energy efficiency as the discharge energy divided by the charge energy. Thus, the voltage efficiency can be calculated by dividing the energy efficiency by the columbic efficiency.

3. Results and discussions

Surface images of a Ti/:IrO_2:Ta_2O_5 electrode at two different magnifications is shown in Fig. 3. The images (Fig. 3a and b) show many cracks on the surface of the coating. The coating is heterogeneous with a "mud-cracked" morphology, containing agglomerates of Ti/:IrO_2:Ta_2O_5 crystals. The formation of these crystal phases is attributed to the epitaxial growth of rutile Ti/:IrO_2:Ta_2O_5 on isomorphous rutile TiO_2 sites, which were formed during substrate etching and/or during the thermal decomposition of the initial coating layers.

Cyclic voltammetry of the graphite and Ti/:IrO_2:Ta_2O_5 electrodes at different scan rates of 5, 20 and 50 mV s^{-1} was carried out using a 1.7 M $V^{3.5+}$ solution containing 4 M H_2SO_4 is shown in Fig. 4. The graphite electrode exhibited an anodic peak at 1.25 V and a corresponding cathodic peak at 0.8 V (Fig. 4a). For the Ti/:IrO_2:Ta_2O_5 electrode, the oxidation and reduction potentials were 1.25 V and 0.75 V, respectively (Fig. 4b). The results indicate that with the Ti/:IrO_2:Ta_2O_5 electrode, the oxidation potential of the V^{+4} to V^{+5} transition occurred (0.72 V) before that of the graphite electrode (0.85 V). When the scan rate was increased from 5 to 50 mV s^{-1}, the peak potential separation for the V^{+4}/V^{+5} redox reaction on both electrodes increased from 1.25 to 1.3 V and the peak current for the V^{+4}/V^{+5} redox reaction were nearly the same for both electrodes. Additionally, the peak potential separation of the V^{2+}/V^{3+} redox reaction was increased from −0.85 V to −0.4 V on the graphite electrode. In the Ti/IrO_2:Ta_2O_5 electrode, the peak potential separations for the V^{3+}/V^{4+} redox reaction were −0.3 V and 0.25 V, beyond which hydrogen evolution took place. The results show that there was no redox couple peak of V^{2+}/V^{3+} on the Ti/IrO_2:Ta_2O_5

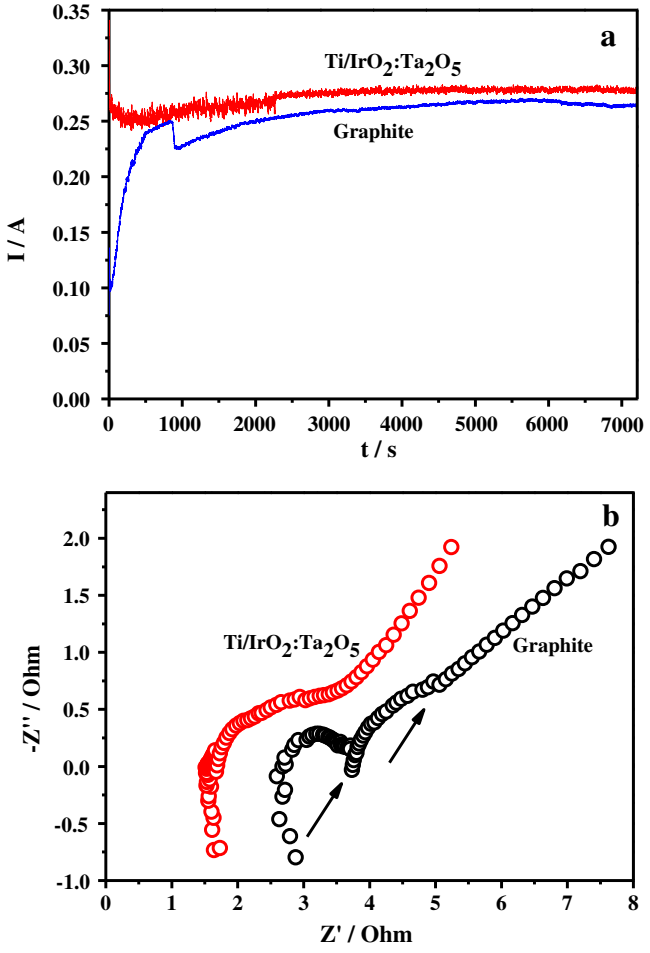

Fig. 5. a: The chronoamperograms of the graphite and Ti/IrO_2:Ta_2O_5 electrodes. b: The electrochemical impedance spectra for the two electrodes at the redox potential of vanadium electrolyte.

electrode, which may due to the catalytic behaviour of Ti/IrO_2:-Ta_2O_5. The formation of a new redox couple, V^{3+}/V^{4+} (Fig. 4c), enhanced the energy density of the vanadium electrolyte, hydrogen evolution suppression and energy efficiency of the VRFB. The oxidation and reduction peak potential of the V^{+4}/V^{+5}, V^{3+}/V^{4+} and V^{+2}/V^{+3} couples experienced slight changes with the scan rate for both the Ti/IrO_2:Ta_2O_5 and graphite electrodes.

The result of chronoamperograms of the graphite and Ti/IrO_2:-Ta2O5 electrode is shown in Fig. 5a. Chronoamperometry was employed to further test the activity of these two electrodes. The electrode potential shifted to the oxidation potential of vanadium in each case. For the Ti/IrO_2:Ta_2O_5 electrode, the steady-state current remained above that of the graphite electrode. For the graphite electrode, erosion (surface modification) began after 25 s. After continuous operation, the current increased due to the formation of a spongy surface on the graphite electrode, which became more porous and thus experienced an increase in surface area. However, for the Ti/IrO_2:Ta_2O_5 and graphite electrodes, constant currents of 0.275 mA and 0.250 mA, respectively, were observed even after 7200 s. Since the electrode Ti/IrO_2:Ta_2O_5 exhibited a better catalytic activity, it can be used as an electrode in practical applications.

Electrochemical impedance spectrum of the electrodes at the redox potential of the vanadium electrolyte is shown in Fig. 5b. The impedance behaviour of the graphite and Ti/IrO_2:Ta_2O_5 electrodes were investigated to understand the kinetics of the electrochemical process that affects the performance of the electrodes when used as high-current-density anodes in vanadium redox flow batteries. Generally, Nyquist plots show one or two semicircles associated with the diffusion of vanadium and the formation of a passive layer on the electrode and other semicircles associated with the charge-transfer resistance and the capacitance at the surface film/anode particle interface. Two semicircles (Fig. 5b) were formed for both electrodes. The Nyquist plots reveal that the R_{ct} (charge transfer resistance) value is significantly lower for the Ti/IrO_2:Ta_2O_5 electrode. In the case of the graphite electrode, a very high R_{ct} value of nearly 5.2 Ω was obtained. For the Ti/IrO_2:Ta_2O_5 electrode, the R_{ct} value was close to 3.1 Ω (The R_{ct} values were calculated by extrapolating the curve to a semicircle and then measuring the diameter of the semicircle). These results indicate that the lower resistance of the Ti/IrO_2:Ta_2O_5 electrode is consistent with the chronoamperometry results, demonstrating the better performance of the Ti/IrO_2:Ta_2O_5 electrode relative to that of the graphite electrode.

Charge–discharge experiments were carried out for the Ti/IrO_2:Ta_2O_5 and graphite electrodes at current densities of 40, 50, 60, 70, 80 and 85 mA cm^{-2}, the results of which are shown in Fig. 6a and b. From the charge–discharge curves, it should be noted that when the current density increases, the voltage efficiency and energy efficiency decrease, but the columbic efficiency increases linearly.

Charge–discharge curves at current densities of 40 and 50 mA cm^{-2} for the Ti/IrO_2:Ta_2O_5 and graphite electrodes are performed and showed in Fig. 6c. In the charge–discharge curves, the VRFB with the Ti/IrO_2:Ta_2O_5 electrode exhibits a larger discharge capacity and discharge energy than those of the VRFB with the graphite electrode due to the former's better catalytic activity and formation of the V^{3+}/V^{4+} redox couple reaction, as verified by CV. The corresponding energy density for the Ti/:IrO_2:Ta_2O_5 and graphite electrodes were 33 Wh L^{-1} and 31.5 Wh L^{-1}, respectively, revealing that the Ti/:IrO_2:Ta_2O_5 electrode can improve the energy density of the VRFB.

The columbic, voltage and energy efficiencies of the charge–discharge performance of the VRFBs with the Ti/IrO_2:Ta_2O_5 and graphite electrodes are shown in Fig. 7a and b. With the graphite

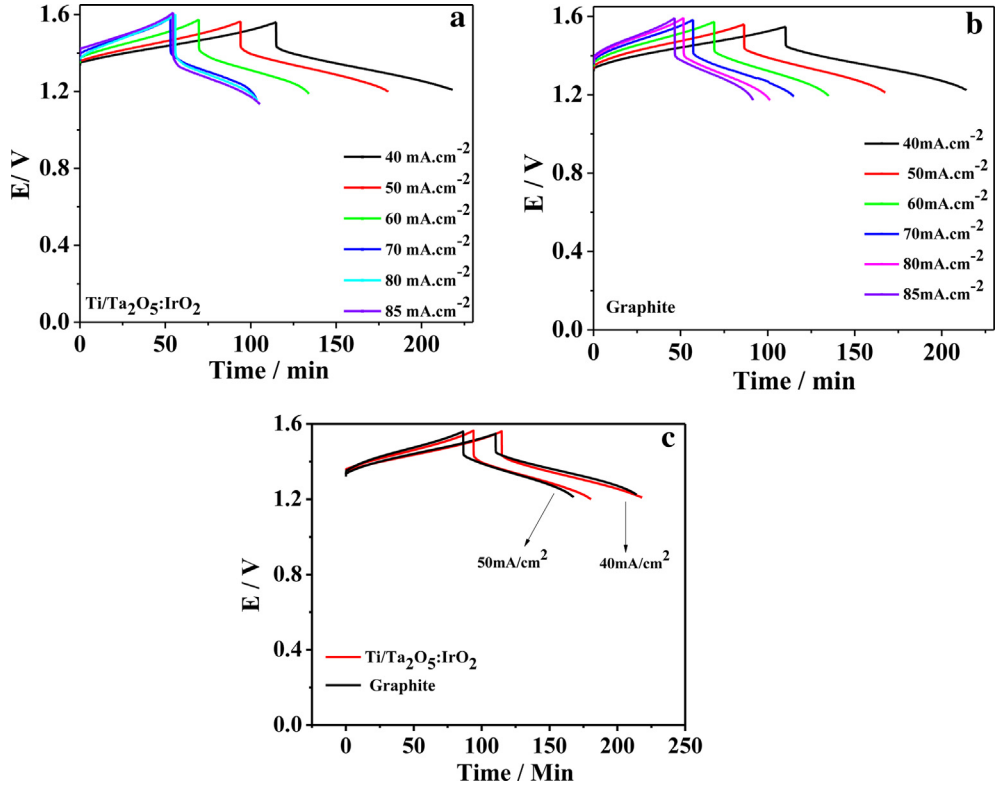

Fig. 6. a and b: The charge–discharge performance of Ti/IrO_2:Ta_2O_5 and graphite electrodes at different current densities. c: The comparison of charge–discharge performances of Ti/IrO_2:Ta_2O_5 and graphite electrodes curves at 40 and 50 mA cm^{-2}.

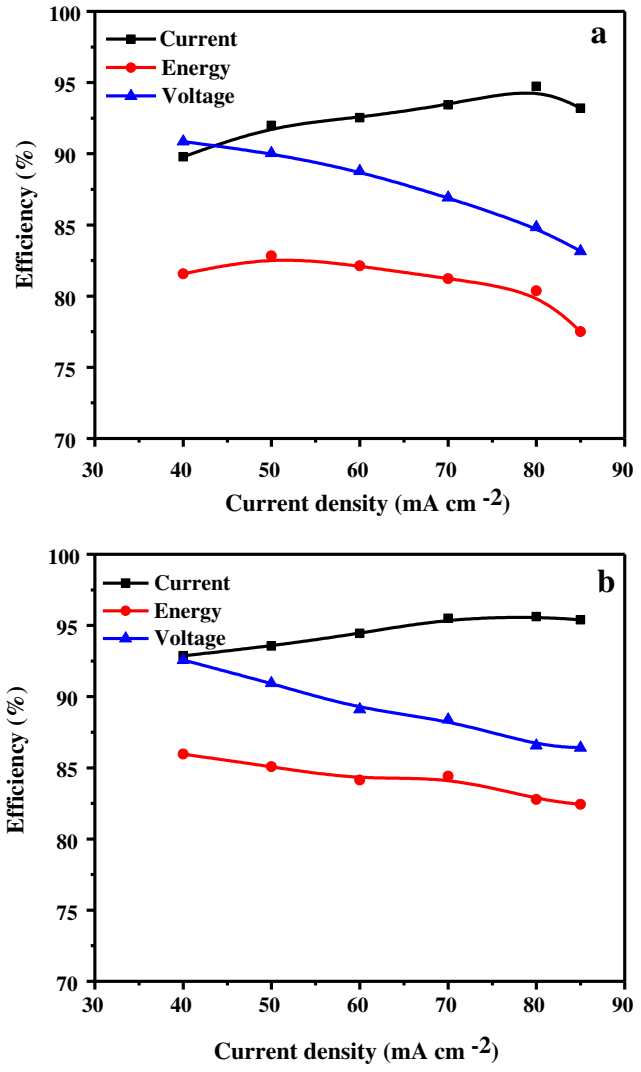

Fig. 7. a and b: Columbic, voltage and energy efficiencies of the VRFB with Ti/IrO_2:-Ta_2O_5 and graphite electrodes, respectively.

electrode, a columbic efficiency of 93%, voltage efficiency of 92.5% and energy efficiency of 86% were achieved at a current density of 40 mA cm^{-2}. For the Ti/:IrO_2:Ta_2O_5 electrode, the columbic efficiency, voltage efficiency and energy efficiency were approximately 90, 91 and 81.5%, respectively. With the increase in the current density, the voltage efficiency and energy efficiency were reduced to some extent. However, even at a high current density of 85 mA cm^{-2}, voltage efficiencies of 86.4% and 83.15% and energy efficiencies of 82.5% and 77.5% were obtained for the graphite and Ti/:IrO_2:Ta_2O_5 electrodes, respectively. The results of this study indicate that the Ti/IrO_2:Ta_2O_5 electrode exhibited lower energy efficiency and voltage efficiency than the graphite electrode due to hydrogen evolution instead of V^{2+} formation at the Ti/IrO_2:Ta_2O_5 electrode, which is substantiated by cyclic voltammetry studies.

4. Conclusions

The present work described the preparation and electrochemical characterisation of Ti/IrO_2:Ta_2O_5 electrodes, whose electrochemical performance is compared with that of a graphite electrode in a vanadium redox flow battery. The CV, chronoamperometry and EIS techniques have been used to investigate the electrochemical properties of the two electrodes. The results show that the electrochemical activity of the Ti/IrO_2:Ta_2O_5 electrode is significantly higher than that of the graphite electrode. The Ti/IrO_2:Ta_2O_5 electrode has a great advantage in the formation of V^{3+}/V^{4+} redox couples. Hence, it showed a much higher energy density (33 Wh L^{-1}) than that of graphite (31.5 Wh L^{-1}) electrode. Lower columbic and energy efficiency have also been observed for the Ti/IrO_2:Ta_2O_5 electrode due to hydrogen evolution.

Acknowledgement

The authors gratefully acknowledge AcRF Tier 1 RG 31/08 of MOE (Singapore), NRF2009EWT-CERP001-026 (Singapore) and the Singapore Ministry of Education (MOE2010-T2-1-017).

References

[1] E. Sum, M. Rychcik, M. Skyllas-Kazacos, J. Power Sources 16 (1985) 85.
[2] M. Kazacos, M. Cheng, M. Skyllas-Kazacos, J. Appl. Electrochem. 20 (1990) 463.
[3] M.S. Skyllas-Kazacos; R.G. Robins, All-vanadium Redox Battery, U.S. Patent No. 4,786,567, 1988.
[4] W. Wang, Z. Nie, B. Chen, F. Chen, Q. Luo, X. Wei, G.G. Xia, M.S. Maria Skyllas-Kazacos, L. Li, Z. Yang, Adv. Energy Mater. 2 (2012) 487.
[5] W. Wang, Q. Luo, B. Li, X. Wei, L. Li, Z. Yang, Adv. Funct. Mater. 23 (2013) 970.
[6] I. Tsuda, K. Nozaki, K. Sakuta, K. Kurokawa, Solar Energy Mater. Sol. Cells 47 (1997) 101.
[7] J. Liu, J. Zhang, Z. Yang, J.P. Lemmon, C. Imhoff, G.L. Graff, L. Li, J. Hu, C. Wang, J. Xiao, G. Xia, V.V. Viswanathan, S. Baskaran, V. Sprenkle, X. Li, Y. Shao, B. Schwenzer, Adv. Funct. Mater. 23 (2013) 929.
[8] M. Gattrell, J. Qian, C. Stewart, P. Graham, B. MacDougall, Electrochim. Acta 51 (2005) 395.
[9] L. Li, S. Kim, W. Wang, M. Vijayakumar, Z. Nie, B. Chen, J. Zhang, G. Xia, J. Hu, G. Graff, J. Liu, Z. Yang, Adv. Energy Mater. 1 (2011) 394.
[10] S. Zhong, C. Padeste, M. Kazacos, M. Skyllas-Kazacos, J. Power Sources 45 (1993) 29.
[11] H. Kaneko, K. Nozaki, Y. Wada, T. Aoki, A. Negishi, M. Kamimoto, Electrochim. Acta 36 (1991) 1191.
[12] B. Sun, M. Skyllas-Kazakos, Electrochim. Acta 36 (1991) 513.
[13] M. Rychcik, M. Skallas-Kazacos, J. Power Sources 19 (1987) 45.
[14] C. Fabjan, J. Garche, B. Harrer, L. Jorissen, C. Kolbeck, F. Philippi, G. Tomazic, Electrochim. Acta 47 (2001) 825.
[15] G. Foti, C. Mousty, V. Reid, C. Comninellis, Electrochim. Acta 44 (1998) 813.
[16] G. Lodi, A.D. Battisti, A. Benedetti, G. Faghazzi, J. Kristof, J. Electroanal. Chem. 256 (1988) 441.
[17] G.W. Jang, K. Rajeshwar, J. Electrochem. Soc. 134 (1987) 1830.
[18] D.M. Novak, B.V. Tilak, B.E. Conway, in: J.O.'M. Bockris, B.E. Conway, White (Eds.), Modern Aspects of Electrochemistry, vol. 14, Plenum Press, New York, 1982, pp. 195–222.
[19] S. Trasatti, G. Buzzanca, J. Electroanal. Chem. 29 (1971) A1.
[20] G.P. Vercesi, J.-Y. Salamin, C.H. Comninellis, Electrochim. Acta 36 (1991) 991.